Available online at www.sciencedirect.com
ScienceDirect
Systems & Control Letters 56 (2007) 245–252
SYSTEMS & CONTROL LETTERS
www.elsevier.com/locate/sysconle

Source seeking with non-holonomic unicycle without position measurement and with tuning of forward velocity

Chunlei Zhang[a], Daniel Arnold[b], Nima Ghods[b], Antranik Siranosian[b], Miroslav Krstic[b,*]

[a]*Department of Electrical and Computer Engineering,University of Dayton, 300 College Park, Dayton, OH 45469, USA*
[b]*Department of Mechanical and Aerospace Engineering, University of California, San Diego, La Jolla, CA 92093-0411, USA*

Received 18 April 2006; received in revised form 18 September 2006; accepted 5 October 2006
Available online 28 November 2006

Abstract

We consider the problem of seeking the source of a scalar signal using an autonomous vehicle modeled as the non-holonomic unicycle and equipped with a sensor of that scalar signal but not possessing the capability to sense either the position of the source nor its own position. We assume that the signal field is the strongest at the source and decays away from it. The functional form of the field is not available to our vehicle. We employ extremum seeking to estimate the gradient of the field in real time and steer the vehicle towards the point where the gradient is zero (the maximum of the field, i.e., the location of the source). We employ periodic forward–backward movement of the unicycle (implementable with mobile robots and some underwater vehicles but not with aircraft), where the forward velocity has a tunable bias term, which is appropriately combined with extremum seeking to produce a net effect of "drifting" towards the source. In addition to simulation results we present a local convergence proof via averaging, which exhibits a delicate periodic structure with two sinusoids of different frequencies—one related to the angular velocity of the unicycle and the other related to the probing frequency of extremum seeking.

Keywords: Extremum seeking; Autonomous agents; Underwater vehicles

1. Introduction

In the rapidly growing literature on coordinated motion control and autonomous agents, "autonomy" never means deprivation of position information. The vehicles are always assumed to have GPS and/or INS on board. There is, however, interest in developing vehicles with full autonomy. The reasons are twofold: (1) applications under water, under ice, or in caves where GPS is unavailable, and (2) the high cost of INS systems that remain accurate over longer periods of time.

In this paper we consider the problem of seeking the source of a scalar signal. One can imagine such signal to be the concentration of a chemical or biological agent, an electromagnetic, acoustic, or even thermal signal. The strength of the signal is assumed to decay away from the source (though not necessarily in a symmetric/concentric pattern), however, the shape of the signal field is not available to the seeking vehicle. The seeking vehicle has access only to the *value* of the signal at its location. In our recent work [18] we considered this problem in the case where the vehicle is modeled by a point mass. In this paper we consider a more challenging (and realistic) model of the vehicle motion—a non-holonomic unicycle. For seeking the source we employ the extremum seeking method which uses non-model-based gradient estimation, where the gradient is estimated using particular motion of the vehicle in space. Motions that allow gradient estimation are much harder to achieve with the unicycle than with a point mass, however, we do succeed in developing a simple and provably stable scheme that drives our kinematically constrained vehicle towards the signal source.

Somewhat related problems have been considered in the past. Porat and Nehorai [16] considered the problem of localizing vapor-emitting sources in spatio-temporal fields modeled by the heat equation PDE, however, their vehicle had position information and could move arbitrarily fast from one point in space to another. Ogren et al. [13] considered coordination problems with groups of vehicles where each vehicle carries a single

* Corresponding author. Tel.: +1 858 822 1374; fax: +1 858 822 3107.
E-mail addresses: zhangchz@notes.udayton.edu (C. Zhang), dbarnold@ucsd.edu (D. Arnold), nghods@ucsd.edu (N. Ghods), asiranosian@ucsd.edu (A. Siranosian), krstic@ucsd.edu (M. Krstic).

0167-6911/$ - see front matter © 2006 Elsevier B.V. All rights reserved.
doi:10.1016/j.sysconle.2006.10.014

sensor and gradient climbing is performed. Gradient estimation in that work is a group effort among vehicles that have position information and communicate amongst themselves.

Unicycle models of autonomous vehicles have been employed in several previous studies of coordinated motion control—by Justh and Krishnaprasad [6] for convergent vehicle formations, by Klein and Morgansen [8] for trajectory tracking, and by Marshall et al. [12] for the cyclic pursuit problem.

The approach we employ for source seeking is the "extremum seeking" method [2] for real-time non-model-based optimization. Extremum seeking, in its various variants, has recently seen several exciting applications [3,14,15,11,19]. The novelty of our result here is in simultaneously solving a non-holonomic steering problem and an adaptive optimization problem. This is achieved with a scheme of utmost simplicity, as evident in Fig. 2. We present a local convergence proof via averaging, which exhibits a delicate periodic structure with two sinusoids of different frequencies—one (slower) related to the angular velocity of the unicycle and the other (faster) related to the probing frequency of extremum seeking. The techniques introduced by Tan et al. [17] can possibly be used to achieve a semi-global version of our result.

2. The model of autonomous vehicle

We consider a unicycle model of a mobile robot with a sensor that is either collocated at the center of the vehicle or mounted some distance r away from the center. A diagram depicting the position, heading, angular and forward velocities, and the sensor location on the autonomous vehicle is shown in Fig. 1. According to the diagram, the equations of motion for the vehicle center are

$$\dot{x}_c = v\cos\theta, \tag{1}$$

$$\dot{y}_c = v\sin\theta, \tag{2}$$

$$\dot{\theta} = \omega_0, \tag{3}$$

where $[x_c, y_c]$ is the center of the vehicle, θ is the orientation, and v, ω_0 are the forward and angular velocity inputs. We point out that our extremum seeking algorithm will be tuning only the forward velocity input v, while keeping the angular velocity input ω_0 constant. The sensor position is governed by the equations

$$\dot{x}_s = v\cos\theta - r\omega_0\sin\theta, \tag{4}$$

$$\dot{y}_s = v\sin\theta + r\omega_0\cos\theta, \tag{5}$$

where $[x_s, y_s]$ is the position of the sensor and r is the distance between the sensor and center of the vehicle. We observe that the relationship between the center of the vehicle and the sensor is

$$x_s = x_c + r\cos\theta, \tag{6}$$

$$y_s = y_c + r\sin\theta. \tag{7}$$

The distance r from the sensor to the center of the vehicle is allowed to be zero in the search approach via extremum seeking. However, in some applications the sensor may be mounted off-center for design reasons. Additionally, the placement of the sensor with $r > 0$ tends to improve the convergence rate because one is "sweeping" the concentration field more broadly with lesser movement of the vehicle itself, yielding better estimation of the gradient. For all the above reasons, we consider the general case $r \geqslant 0$ in our analysis.

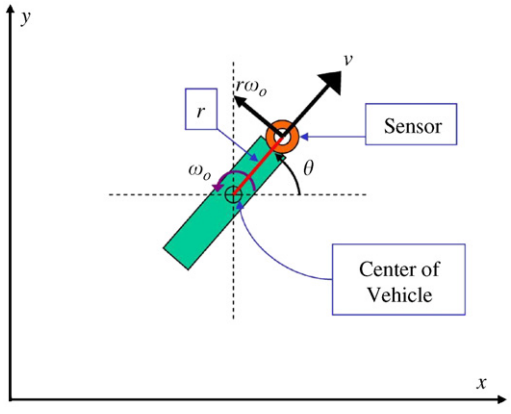

Fig. 1. Unicycle model with non-collocated sensor.

3. The search algorithm via extremum seeking

We assume that the signal source being tracked is distributed according to an *unknown* nonlinear map $J = f(x, y)$, which has an isolated local maximum $f^* = f(x^*, y^*)$ at (x^*, y^*). Our purpose is to control the autonomous vehicle to achieve local convergence to the maximizer (x^*, y^*) without the knowledge of the shape of $f(x, y)$ and using only the measurements of its value during the motion of the vehicle.

If we know the nonlinear function $f(x, y)$ and if we can directly actuate (and measure) the position of the vehicle, then we can design a control law to force the vehicle's motion to evolve according to the gradient dynamical system

$$[\dot{x}_c, \dot{y}_c]^\top = -\nabla f(x_c, y_c).$$

In that case the trajectory of $[x_c, y_c]$ will asymptotically converge to the set of stationary points of f where $\nabla f(x^*, y^*) = 0$. Even finite time tracking can be obtained with the gradient system

$$[\dot{x}_c, \dot{y}_c]^\top = -\frac{\nabla f(x_c, y_c)}{\|\nabla f(x_c, y_c)\|_2},$$

as explained by Cortes [5].

In the absence of the knowledge of function $f(x, y)$ and of the vehicle's position, we have to employ techniques of non-model-based optimization. In addition, in the absence of direct actuation of the vehicle's position, namely, for a non-holonomic vehicle that cannot be directly steered sideways and all of its motion has to be produced using forward and angular velocity inputs, the task of source seeking becomes even more challenging.

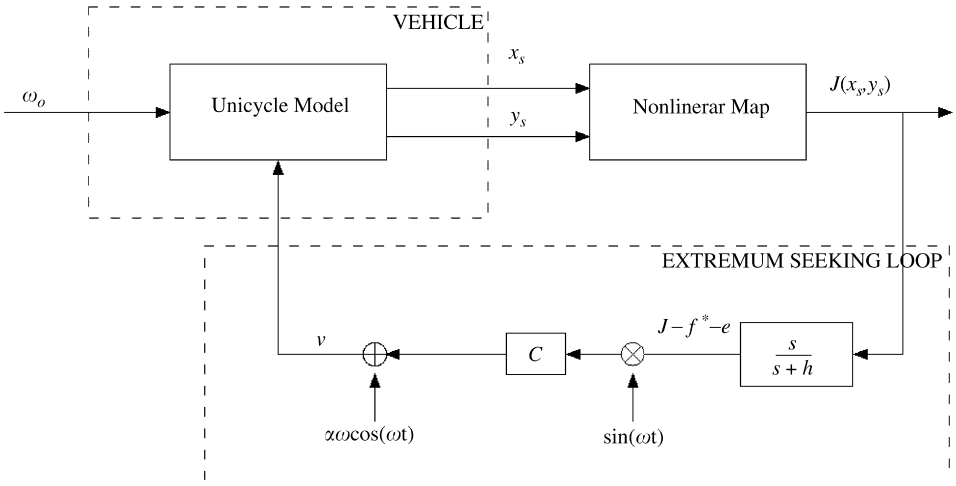

Fig. 2. Extremum seeking for unicycle model.

In this paper, given only the measurement of the values of the function $J = f(x_s, y_s)$, we employ extremum seeking to tune the forward velocity v (with fixed angular velocity ω_0) to ensure that $[x_c(t), y_c(t)]$ asymptotically converges towards $[x^*, y^*]$. A block diagram of the extremum seeking scheme is shown in Fig. 2. The designer can affect the seeking performance using the parameters α, ω, ω_0, and c.

4. Stability analysis

For clarity of our presentation, we assume that the nonlinear map is quadratic and that its Hessian is diagonal, viz.,

$$J = f(x, y) = f^* - q_x(x - x^*)^2 - q_y(y - y^*)^2, \tag{8}$$

where (x^*, y^*) is the maximizer, $f^* = f(x^*, y^*)$ is the maximum and q_x, q_y are some unknown positive constants (since the Hessian is negative). General non-quadratic maps with non-diagonal Hessians are equally amenable to analysis, using the same technique as in [2,9].

By fixing the angular velocity to be ω_0, we have $\theta = \omega_0 t$. Moreover, we set the perturbation frequency $\omega = k\omega_0$ for a positive integer $k > 3$. The analysis that follows employs the method of averaging. Let

$$e = \frac{h}{s+h}[J] - f^*, \tag{9}$$

then the signal after the washout filter $s/(s + h)$ in Fig. 2 can be expressed as

$$\Delta = \frac{s}{s+h}[J] = J - \frac{h}{s+h}[J] = J - f^* - e.$$

Now, let us introduce new coordinates

$$\tilde{x} = x_s - x^* - \alpha\sin(\omega t)\cos(\omega_0 t) - r\cos(\omega_0 t), \tag{10}$$
$$\tilde{y} = y_s - y^* - \alpha\sin(\omega t)\sin(\omega_0 t) - r\sin(\omega_0 t). \tag{11}$$

Then, in the time scale $\tau = \omega t$, we have

$$\begin{aligned}
\frac{\mathrm{d}\tilde{x}}{\mathrm{d}\tau} &= \frac{1}{\omega}\frac{\mathrm{d}\tilde{x}}{\mathrm{d}t} \\
&= \frac{1}{\omega}[v\cos(\omega_0 t) - r\omega_0\sin(\omega_0 t) - \alpha\omega\cos(\omega t)\cos(\omega_0 t) \\
&\quad + \alpha\omega_0\sin(\omega t)\sin(\omega_0 t) + r\omega_0\sin(\omega_0 t)] \\
&= \frac{1}{\omega}[c\sin(\omega t)\cos(\omega_0 t)\Delta + \alpha\omega\cos(\omega t)\cos(\omega_0 t) \\
&\quad - \alpha\omega\cos(\omega t)\cos(\omega_0 t) + \alpha\omega_0\sin(\omega t)\sin(\omega_0 t)] \\
&= \frac{1}{\omega}[c\sin\tau\cos(\tau/k)\Delta + \alpha\omega_0\sin\tau\sin(\tau/k)],
\end{aligned}$$

$$\begin{aligned}
\frac{\mathrm{d}\tilde{y}}{\mathrm{d}\tau} &= \frac{1}{\omega}\frac{\mathrm{d}\tilde{y}}{\mathrm{d}t} \\
&= \frac{1}{\omega}[v\sin(\omega_0 t) + r\omega_0\cos(\omega_0 t) - \alpha\omega\cos(\omega t)\sin(\omega_0 t) \\
&\quad - \alpha\omega_0\sin(\omega t)\cos(\omega_0 t) - r\omega_0\cos(\omega_0 t)] \\
&= \frac{1}{\omega}[c\sin(\omega t)\sin(\omega_0 t)\Delta + \alpha\omega\cos(\omega t)\sin(\omega_0 t) \\
&\quad - \alpha\omega\cos(\omega t)\sin(\omega_0 t) - \alpha\omega_0\sin(\omega t)\cos(\omega_0 t)] \\
&= \frac{1}{\omega}[c\sin\tau\sin(\tau/k)\Delta - \alpha\omega_0\sin\tau\cos\tau/k)],
\end{aligned}$$

$$\frac{\mathrm{d}e}{\mathrm{d}\tau} = \frac{1}{\omega}\frac{\mathrm{d}e}{\mathrm{d}t} = \frac{h}{\omega}\Delta,$$

where

$$\begin{aligned}
\Delta = &-q_x(\tilde{x} + \alpha\sin\tau\cos(\tau/k) + r\cos(\tau/k))^2 \\
&- q_y(\tilde{y} + \alpha\sin\tau\sin(\tau/k) + r\sin(\tau/k))^2 - e.
\end{aligned} \tag{12}$$

So we summarize the system in Fig. 2 for the unicycle with non-collocated sensor as

$$\frac{\mathrm{d}\tilde{x}}{\mathrm{d}\tau} = \frac{1}{\omega}[c\sin\tau\cos(\tau/k)\Delta + \alpha\omega_0\sin\tau\sin(\tau/k)], \tag{13}$$

$$\frac{\mathrm{d}\tilde{y}}{\mathrm{d}\tau} = \frac{1}{\omega}[c\sin\tau\sin(\tau/k)\Delta - \alpha\omega_0\sin\tau\cos(\tau/k)], \tag{14}$$

$$\frac{\mathrm{d}e}{\mathrm{d}\tau} = \frac{h}{\omega}\Delta. \tag{15}$$

System (13)–(15) is in the form to which the averaging method is applicable, provided $1/\omega$ is small, i.e., provided ω is large (relative to the other parameters in the extremum seeking scheme and relative to the parameters in the nonlinear map). Now, averaging (13)–(15) over the larger period $2\pi k$, we have

$$\begin{aligned}
\frac{\mathrm{d}\tilde{x}_{\mathrm{avg}}}{\mathrm{d}\tau} &= \frac{1}{\omega}\frac{1}{2k\pi}\int_0^{2k\pi}\frac{\mathrm{d}\tilde{x}}{\mathrm{d}t}\,\mathrm{d}\tau \\
&= \frac{1}{\omega}\frac{1}{2k\pi}\int_0^{2k\pi}[c\sin\tau\cos(\tau/k)\Delta+\alpha\omega_0\sin\tau\sin(\tau/k)]\,\mathrm{d}\tau \\
&= \frac{1}{\omega}\frac{1}{2\pi}\int_0^{2\pi}[c\sin(k\tau)\cos\tau\Delta + \alpha\omega_0\sin(k\tau)\sin\tau]\,\mathrm{d}\tau \\
&= \frac{1}{\omega}\frac{1}{2\pi}\Bigg\{-\int_0^{2\pi}c\sin(k\tau)\cos\tau(q_x\tilde{x}^2+q_y\tilde{y}^2+e)\,\mathrm{d}\tau \\
&\quad -\int_0^{2\pi}c\sin(k\tau)\cos\tau[2q_x\tilde{x}\alpha\sin(k\tau)\cos\tau \\
&\quad +2q_x\tilde{x}r\cos\tau+2q_x\alpha r\sin(k\tau)\cos^2\tau \\
&\quad +2q_y\tilde{y}\alpha\sin(k\tau)\sin\tau+2q_y\tilde{y}r\sin\tau \\
&\quad +2q_y\alpha r\sin(k\tau)\sin^2\tau]\,\mathrm{d}\tau \\
&\quad -\int_0^{2\pi}c\sin(k\tau)\cos\tau[q_x\alpha^2\sin^2(k\tau)\cos^2\tau \\
&\quad +q_xr^2\cos^2\tau+q_y\alpha^2\sin^2(k\tau)\sin^2\tau \\
&\quad +q_yr^2\sin^2\tau]\,\mathrm{d}\tau \\
&\quad +\int_0^{2\pi}\alpha\omega_0\sin(k\tau)\sin\tau\,\mathrm{d}\tau\Bigg\} \\
&= -\frac{1}{\omega}\frac{1}{2\pi}\frac{\pi}{2}c2q_x\tilde{x}_{\mathrm{avg}}\alpha \\
&= -\frac{1}{2\omega}\alpha cq_x\tilde{x}_{\mathrm{avg}},
\end{aligned}$$

$$\begin{aligned}
\frac{\mathrm{d}\tilde{y}_{\mathrm{avg}}}{\mathrm{d}\tau} &= \frac{1}{\omega}\frac{1}{2k\pi}\int_0^{2k\pi}\frac{\mathrm{d}\tilde{y}}{\mathrm{d}t}\,\mathrm{d}\tau \\
&= \frac{1}{\omega}\frac{1}{2k\pi}\int_0^{2k\pi}[c\sin\tau\sin(\tau/k)\Delta-\alpha\omega_0\sin\tau\cos(\tau/k)]\,\mathrm{d}\tau \\
&= \frac{1}{\omega}\frac{1}{2\pi}\int_0^{2\pi}[c\sin(k\tau)\sin\tau\Delta - \alpha\omega_0\sin(k\tau)\cos\tau]\,\mathrm{d}\tau \\
&= \frac{1}{\omega}\frac{1}{2\pi}\Bigg\{-\int_0^{2\pi}c\sin(k\tau)\sin\tau(q_x\tilde{x}^2+q_y\tilde{y}^2+e)\,\mathrm{d}\tau \\
&\quad -\int_0^{2\pi}c\sin(k\tau)\sin\tau[2q_x\tilde{x}\alpha\sin(k\tau)\cos\tau \\
&\quad +2q_x\tilde{x}r\cos\tau+2q_x\alpha r\sin(k\tau)\cos^2\tau \\
&\quad +2q_y\tilde{y}\alpha\sin(k\tau)\sin\tau+2q_y\tilde{y}r\sin\tau \\
&\quad +2q_y\alpha r\sin(k\tau)\sin^2\tau]\,\mathrm{d}\tau \\
&\quad -\int_0^{2\pi}c\sin(k\tau)\sin\tau[q_x\alpha^2\sin^2(k\tau)\cos^2\tau \\
&\quad +q_xr^2\cos^2\tau+q_y\alpha^2\sin^2(k\tau)\sin^2\tau \\
&\quad +q_yr^2\sin^2\tau]\,\mathrm{d}\tau \\
&\quad -\int_0^{2\pi}\alpha\omega_0\sin(k\tau)\cos\tau\,\mathrm{d}\tau\Bigg\} \\
&= -\frac{1}{\omega}\frac{1}{2\pi}\frac{\pi}{2}c2q_y\tilde{y}_{\mathrm{avg}}\alpha \\
&= -\frac{1}{2\omega}\alpha cq_y\tilde{y}_{\mathrm{avg}},
\end{aligned}$$

$$\begin{aligned}
\frac{\mathrm{d}\tilde{e}_{\mathrm{avg}}}{\mathrm{d}\tau} &= \frac{1}{\omega}\frac{1}{2k\pi}\int_0^{2k\pi}\frac{\mathrm{d}\tilde{e}}{\mathrm{d}t}\,\mathrm{d}\tau \\
&= \frac{h}{\omega}\frac{1}{2k\pi}\int_0^{2k\pi}\Delta\,\mathrm{d}\tau \\
&= \frac{h}{\omega}\frac{1}{2\pi}\Bigg\{-\int_0^{2\pi}(q_x\tilde{x}^2+q_y\tilde{y}^2+e)\,\mathrm{d}\tau \\
&\quad -\int_0^{2\pi}[2q_x\tilde{x}\alpha\sin(k\tau)\cos\tau+2q_x\tilde{x}r\cos\tau \\
&\quad +2q_x\alpha r\sin(k\tau)\cos^2\tau+2q_y\tilde{y}\alpha\sin(k\tau)\sin\tau \\
&\quad +2q_y\tilde{y}r\sin\tau+2q_y\alpha r\sin(k\tau)\sin^2\tau]\,\mathrm{d}\tau \\
&\quad -\int_0^{2\pi}[q_x\alpha^2\sin^2(k\tau)\cos^2\tau+q_xr^2\cos^2\tau \\
&\quad +q_y\alpha^2\sin^2(k\tau)\sin^2\tau+q_yr^2\sin^2\tau]\,\mathrm{d}\tau\Bigg\} \\
&= -\frac{h}{\omega}\Bigg[q_x\tilde{x}^2_{\mathrm{avg}}+q_y\tilde{y}^2_{\mathrm{avg}}+e_{\mathrm{avg}} \\
&\quad +\frac{1}{2\pi}\frac{\pi}{2}q_x\alpha^2+\frac{1}{2\pi}\pi q_xr^2+\frac{1}{2\pi}\frac{\pi}{2}q_y\alpha^2+\frac{1}{2\pi}\pi q_yr^2\Bigg] \\
&= -\frac{h}{\omega}\left[q_x\tilde{x}^2_{\mathrm{avg}}+q_y\tilde{y}^2_{\mathrm{avg}}+e_{\mathrm{avg}}+\left(\frac{\alpha^2}{4}+\frac{r^2}{2}\right)(q_x+q_y)\right].
\end{aligned}$$

Then, summarizing the average model we have

$$\frac{\mathrm{d}\tilde{x}_{\mathrm{avg}}}{\mathrm{d}\tau} = -\frac{1}{2\omega}\alpha cq_x\tilde{x}_{\mathrm{avg}}, \tag{16}$$

$$\frac{\mathrm{d}\tilde{y}_{\mathrm{avg}}}{\mathrm{d}\tau} = -\frac{1}{2\omega}\alpha cq_y\tilde{y}_{\mathrm{avg}}, \tag{17}$$

$$\frac{\mathrm{d}e_{\mathrm{avg}}}{\mathrm{d}\tau} = -\frac{h}{\omega}\left[q_x\tilde{x}^2_{\mathrm{avg}}+q_y\tilde{y}^2_{\mathrm{avg}}+e_{\mathrm{avg}}+\left(\frac{\alpha^2}{4}+\frac{r^2}{2}\right)(q_x+q_y)\right]. \tag{18}$$

The equilibrium of the average model (16)–(18) is

$$\tilde{x}^e_{\mathrm{avg}} = 0, \quad \tilde{y}^e_{\mathrm{avg}} = 0, \quad e^e_{\mathrm{avg}} = -\left(\frac{\alpha^2}{4}+\frac{r^2}{2}\right)(q_x+q_y). \tag{19}$$

The Jacobian of (16)–(18) at $(\tilde{x}^e_{\text{avg}}, \tilde{y}^e_{\text{avg}}, e^e_{\text{avg}})$ is

$$J_{\text{avg}} = \frac{1}{\omega}\begin{bmatrix} -\alpha c q_x/2 & 0 & 0 \\ 0 & -\alpha c q_y/2 & 0 \\ 0 & 0 & -h \end{bmatrix}. \tag{20}$$

Given the knowledge that the extremum is a maximum, it follows that q_x, q_y are known to be positive, though their actual values are unknown. Therefore, if we choose $\alpha > 0$, $c > 0$, and $h > 0$, Jacobian (20) is Hurwitz and equilibrium (19) of the average system (16)–(18) is locally exponentially stable. Then according to the averaging theorem [7], we have the following result.

Theorem 4.1. *There exists $\bar{\omega}$ such that for all $1/\omega \in (0, 1/\bar{\omega})$ the system in Fig. 2 has a unique exponentially stable periodic solution $(\tilde{x}^{2\pi/\omega}, \tilde{y}^{2\pi/\omega}, e^{2\pi/\omega})$ of period $2\pi/\omega$ and this solution satisfies*

$$\left\| \begin{bmatrix} \tilde{x}^{2\pi/\omega} \\ \tilde{y}^{2\pi/\omega} \\ e^{2\pi/\omega} + \left(\frac{\alpha^2}{4} + \frac{r^2}{2}\right)(q_x + q_y) \end{bmatrix} \right\| \leqslant O(1/\omega), \quad \forall \tau \geqslant 0. \tag{21}$$

Since

$$\begin{aligned} x_s - x^* &= \tilde{x} + \alpha \sin(\omega t)\cos(\omega_0 t) + r\cos(\omega_0 t) \\ &= \left(\tilde{x} - \tilde{x}^{2\pi/\omega}\right) + \tilde{x}^{2\pi/\omega} + \alpha \sin(\omega t)\cos(\omega_0 t) \\ &\quad + r\cos(\omega_0 t), \end{aligned}$$

the above theorem implies that the first term converges to zero, the second term is $O(1/\omega)$, the third term is $O(\alpha)$ and the forth term is $O(r)$. Thus

$$\limsup_{\tau \to \infty} |x_s - x^*| = O(\alpha + 1/\omega + r).$$

Similarly, we obtain

$$\limsup_{\tau \to \infty} |y_s - y^*| = O(\alpha + 1/\omega + r).$$

Hence, we have

$$\limsup_{\tau \to \infty} |f(x_s, y_s) - f^*| = O(\alpha^2 + (1/\omega)^2 + r^2).$$

The above limits characterize the asymptotic performance of the extremum seeking loop in Fig. 2. The vehicle converges to neighborhood of the maximizer $[x^*, y^*]$, the size of which is proportional to the amplitude of the periodic perturbation, the reciprocal of the perturbation frequency and the vehicle radius. Since we choose α and r as small and ω as large, the tracking error between the vehicle and the source is small. A direct trade-off between the tracking error and the speed of convergence is evident from the fact that two of the eigenvalues of the Jacobian become more negative as α increases.

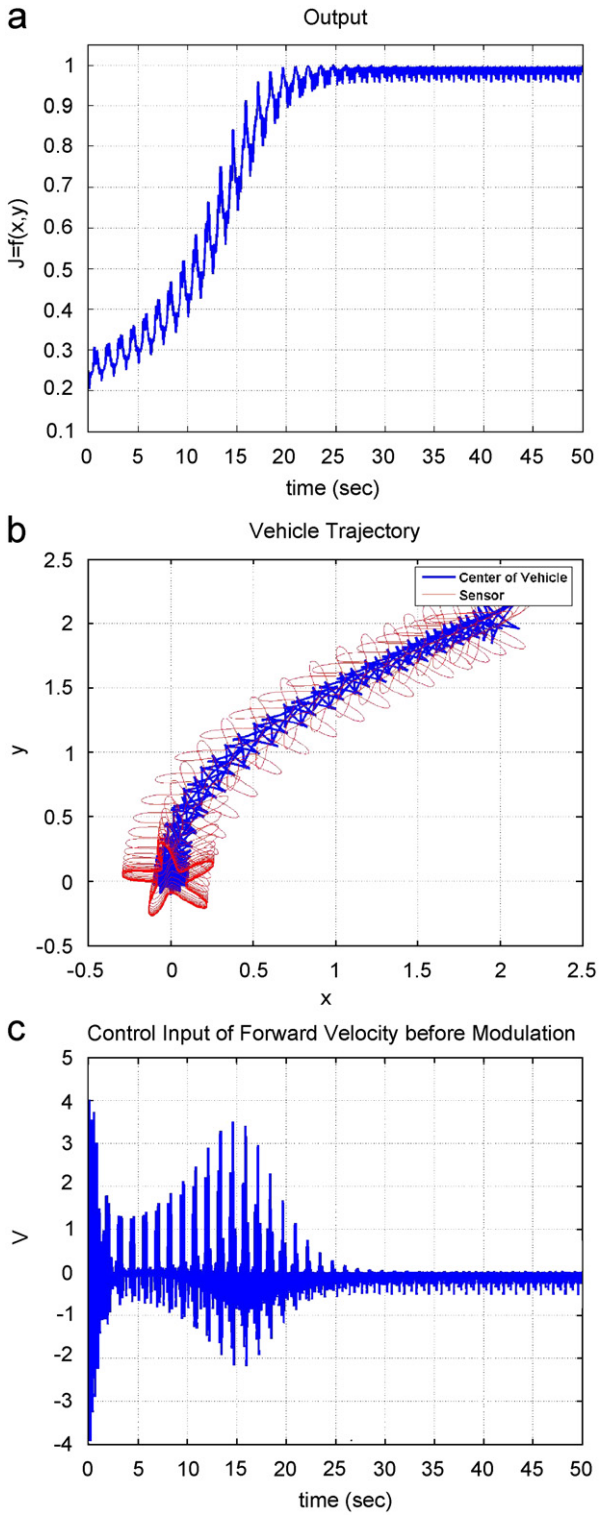

Fig. 3. Extremum seeking of unicycle with non-collocated sensor, stationary target case, $\omega_0 = \omega/5$. (a) Output of nonlinear map; (b) vehicle center and sensor trajectories; (c) forward velocity before modulation.

5. Simulation results

In the following simulations, we set the parameters of the stationary source as $[x^*, y^*] = [0, 0]$, $f^* = 1$, $q_x = 0.5$ and $q_y = 0.25$. The parameters of the extremum seeking loop are chosen as $\omega = 25$, $\alpha = 0.1$, $c = 20$, $h = 1$, and $\omega_0 = \omega/5$. The starting position of the autonomous vehicle is $[x_s(0), y_s(0)] = [2, 2]$, r=0.2, θ_0=π, and therefore $[x_c, y_c]$=[1.8, 2]. As shown

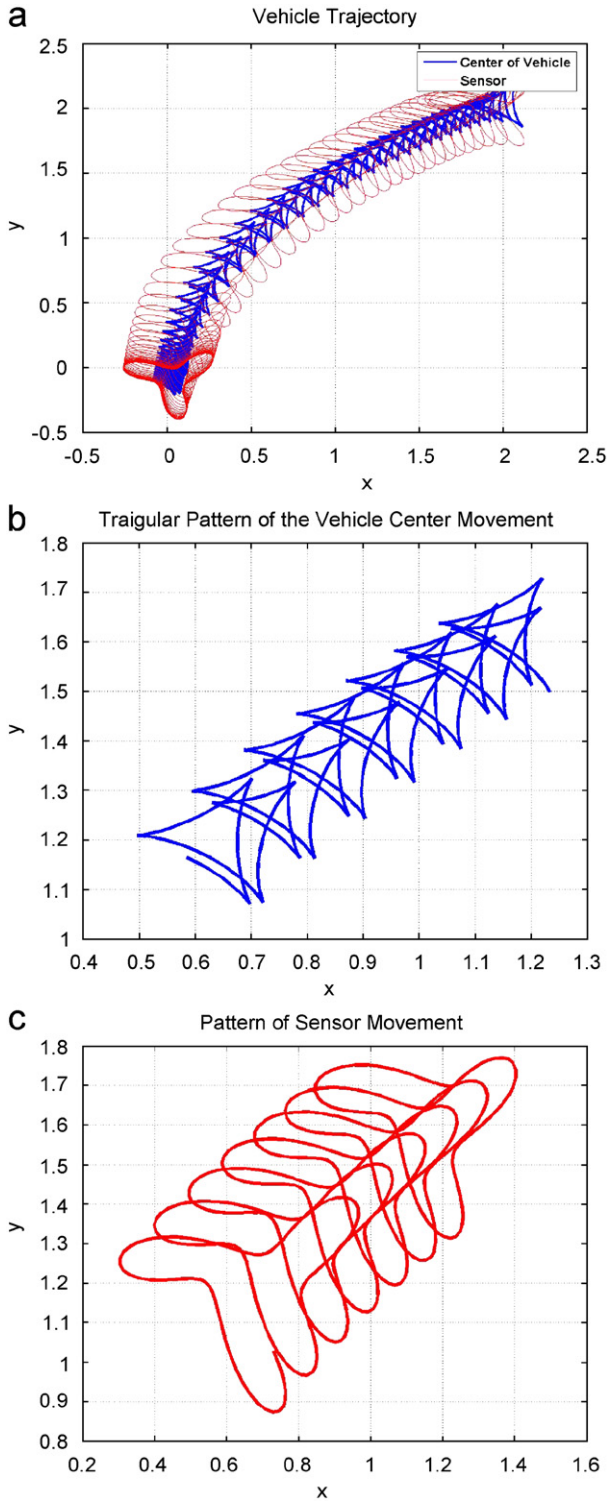

Fig. 4. Extremum seeking of unicycle with non-collocated sensor, stationary target case, $\omega_0 = \omega/3$. (a) Vehicle center and sensor trajectories; (b) triangular pattern of the vehicle center movement; (c) sensor position trajectory.

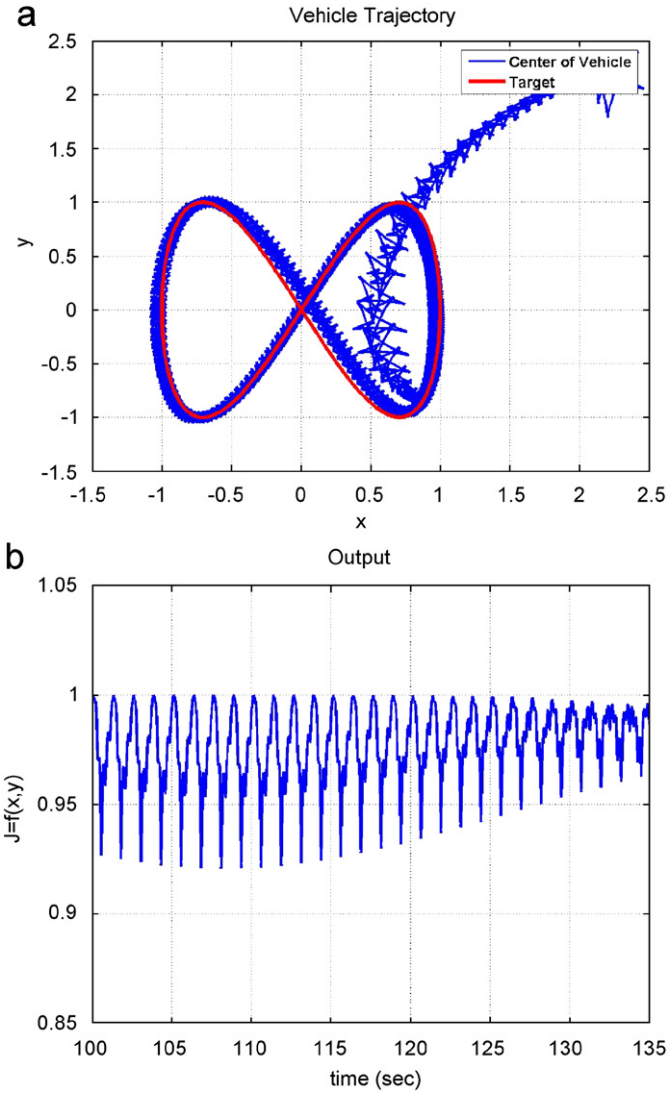

Fig. 5. Moving target. Extremum seeking of unicycle with non-collocated sensor and $\omega_0 = \omega/5$. (a) Vehicle center and target trajectories; (b) output of the nonlinear map.

in Fig. 3(b), the autonomous vehicle starts at [1.8, 2] by probing around to climb the gradient of the unknown map in a star pattern, eventually circling around the maximizer [0, 0]. The output of the unknown signal $J = f(x_s, y_s)$ is shown in Fig. 3(a), while the forward velocity before modulation v is shown in Fig. 3(c). The trajectories of the vehicle center and sensor are compared in Fig. 3(b). Because of the vehicle radius, the steady state position of the sensor forms a star pattern with the vertex nearly 0.2 away from the maximizer [0, 0]. Therefore, the observations from the simulation coincide with the theoretical analysis presented above.

The reason we observe a star pattern with five vertices in the vehicle trajectory (Fig. 3(b)) is due to the scaling constant k. In this case $\omega_0 = \omega/5$. If we change $\omega_0 = \omega/3$, we observe a triangular pattern in the trajectory of the vehicle center, and a star pattern with three vertices in the trajectory of the sensor, refer to Fig. 4.

Finally, we consider a slow moving source whose trajectory is in the shape of the number 8, that is, $x^* = a_m \sin(\omega_m t)$, $y^* = a_m \sin(2\omega_m t)$, where $\omega_m \ll \omega$, the initial position of the target is [0, 0], and $a_m = 1$, $\omega_m = 0.03$. Here, we maintain the

same parameter settings as in the above simulations, except $\alpha = 0.04$, $c = 50$, and $\omega_0 = \omega/5$. The simulation results in Fig. 5 show successful tracking in a non-stationary case.

6. Conclusions

The star- or triangle-patterned motion of our vehicle is perhaps the most interesting part of our result. The gradient is being estimated due to the local exploration of space in a pattern that our kinematically constrained vehicle can execute. Though such motion may appear a little awkward, it should not be entirely surprising because it has come up in motion planning problems for non-holonomic systems such as the "snakeboard," see the work by Lewis et al. [10] and by Bullo and Lewis [4].

The star patterned motion does not seem like the most energy efficient way to move around in space, however, an even bigger problem is that it requires motion both forward and in reverse. As such, it is implementable by mobile robots, ground vehicles, and some underwater vehicles, but not by aircraft. Our future work will deal with an approach dual to the approach in this paper—the forward velocity will be held constant and the angular velocity will be tuned.

We plan on performing experiments with the scheme presented in the present paper.[1] The mobile robot in Fig. 6 is equipped with a light sensor and will be made to seek the extremum on a large printed paper surface, produced on a plotter, and blending smoothly in color from white in the center to gray to black away from the center, as shown in Fig. 7. Our mobile robot is not a unicycle. The motion of its two wheels will be scheduled (in the same or in the opposite direction) to produce arbitrary forward and angular velocities, similar to what is done for the "Caltech hovercraft" [1].

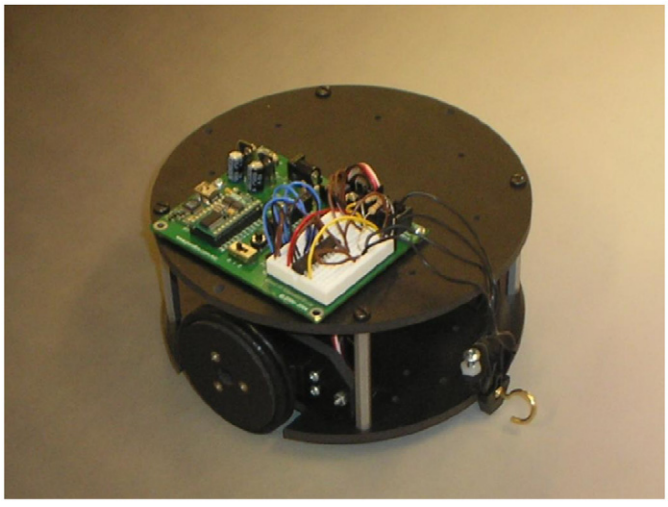

Fig. 6. A two-wheel autonomous vehicle for future experiments.

[1] This implementation, along with an implementation of a future scheme that tunes the angular velocity, will be the subject of a future paper that will be submitted to an applications-oriented journal.

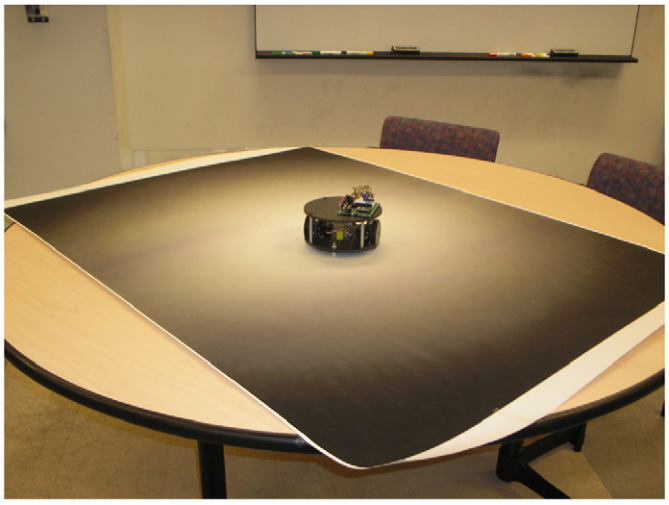

Fig. 7. The mobile robot in Fig. 6 will be made to seek the extremum on a printed paper surface, which varies in color from white in the center to gray to black away from the center.

Acknowledgments

We thank Sonia Martinez for helpful discussions on the literature on coordinated motion control and source seeking.

References

[1] A.P. Aguiar, L. Cremean, J.P. Hespanha, Position tracking for a nonlinear underactuated hovercraft: controller design and experimental results, 2003 IEEE Conference on Decision and Control, 2003.
[2] K.B. Ariyur, M. Krstić, Real-Time Optimization by Extremum-Seeking Control, Wiley-Interscience, Hoboken, NJ, 2003.
[3] A. Banaszuk, S. Narayanan, Y. Zhang, Adaptive control of flow separation in a planar diffuser, Paper AIAA-2003-0617, 41st Aerospace Sciences Meeting & Exhibit, January 2003, Reno NV.
[4] F. Bullo, A.D. Lewis, Kinematic controllability and motion planning for the snakeboard, IEEE Trans. Robotics and Automation 19 (2003) 494–498.
[5] J. Cortés, Achieving coordination tasks in finite time via nonsmooth gradient flows, in: Proceedings of the 2005 IEEE Conference on Decision and Control, 2005.
[6] E.W. Justh, P.S. Krishnaprasad, Equilibria and steering laws for planar formations, Systems Control Lett. 52 (2004) 25–38.
[7] H.K. Khalil, Nonlinear Systems, Prentice-Hall, Englewood Cliffs, NJ, 2001.
[8] D.J. Klein, K.A. Morgansen, Controlled collective motion for trajectory tracking, 2006 American Control Conference, 2006.
[9] M. Krstić, H.-H. Wang, Design and stability analysis of extremum seeking feedback for general nonlinear systems, Automatica 36 (2) (2000) 595–601.
[10] A. Lewis, J. Ostrowski, R. Murray, J. Burdick, Nonholonomic mechanics and locomotion: the snakeboard example, 1994 International Conference on Robotics and Automation, 1994.
[11] Y. Li, M.A. Rotea, G.T.-C. Chiu, L.G. Mongeau, I.-S. Paek, Extremum seeking control of a tunable thermoacoustic cooler, IEEE Trans. Control Systems Technol. 13 (2005) 527–536.
[12] J.A. Marshall, M.E. Broucke, B.A. Francis, Pursuit formations of unicycles, Automatica 42 (2006) 3–12.
[13] P. Ogren, E. Fiorelli, N.E. Leonard, Cooperative control of mobile sensor networks: adaptive gradient climbing in a distributed environment, IEEE Trans. Automat. Control 29 (2004) 1292–1302.
[14] K. Peterson, A. Stefanopoulou, Extremum seeking control for soft landing of an electromechanical valve actuator, Automatica (2004) 1063–1069.

[15] D. Popovic, M. Jankovic, S. Manger, A.R. Teel, Extremum seeking methods for optimization of variable cam timing engine operation, in: Proceedings American Control Conference, Denver, CO, USA, 2003, pp. 3136–3141.
[16] B. Porat, A. Neohorai, Localizing vapor-emitting sources by moving sensors, IEEE Trans. Signal Process. 44 (1996) 1018–1021.
[17] Y. Tan, D. Nesic, I. Mareels, On non-local stability properties of extremum seeking control, in: Proceedings of the 16th IFAC World Congress, 2005.
[18] C. Zhang, A. Siranosian, M. Krstic, Extremum seeking for moderately unstable systems and for autonomous vehicle target tracking without position measurements, 2006 American Control Conference, 2006.
[19] X.T. Zhang, D.M. Dawson, W.E. Dixon, B. Xian, Extremum seeking nonlinear controllers for a human exercise machine, in: Proceedings of the 2004 IEEE Conference on Decision and Control, 2004.